Preprints.org

Temperature-Enhanced Exciton Emission from GaAs Cone-Shell Quantum Dots

Christian Heyn [*] , Leonardo Ranasinghe , Kristian Deneke , Ahmed Alshaikh , Robert Blick

Article

Temperature-Enhanced Exciton Emission from GaAs Cone-Shell Quantum Dots

Christian Heyn *[ORCID], **Leonardo Ranasinghe, Kristian Deneke, Ahmed Alshaikh and Robert H. Blick**

Center for Hybrid Nanostructures (CHyN), University of Hamburg, Luruper Chaussee 149, 22761 Hamburg, Germany

* Correspondence: heyn@physnet.uni-hamburg.de

Abstract: The temperature-dependent intensities of the exciton (X) and biexciton (XX) peaks from single GaAs cone-shell quantum dots (QDs) are studied with micro photoluminescence (PL) at varied excitation power and QD size. The QDs are fabricated by filling of self-assembled nanoholes, which are drilled in an AlGaAs barrier by local droplet etching (LDE) during molecular beam epitaxy (MBE). This method allows the fabrication of strain-free QDs with sizes precisely controlled by the amount of material deposited for hole filling. Starting from the base temperature $T = 3.2$ K of the cryostat, single-dot PL measurements demonstrate a strong enhancement of the exciton emission up to a factor of five with increasing T. Both, the maximum exciton intensity and the temperature $T_{x,max}$ of the maximum intensity depend on excitation power and dot size. At an elevated excitation power, $T_{x,max}$ becomes larger than 30 K. This allows an operation using an inexpensive and compact Stirling cryocooler. Above $T_{x,max}$, the exciton intensity decreases strongly up to its disappearance. The experimental data are quantitatively reproduced by a model which considers the competing processes of exciton generation, annihilation, and recombination. Exciton generation in the QDs is given by the sum of direct excitation in the dot plus additional bulk excitons diffusing from the barrier layers into the dot. The thermally-driven bulk-exciton diffusion from the barriers causes the temperature enhancement of the exciton emission. Above $T_{x,max}$, the intensity decreases due to exciton annihilation processes. In comparison to the exciton, the biexciton intensity shows an only very weak enhancement, which is attributed to more efficient annihilation processes.

Keywords: quantum dot; photoluminescence; exciton; biexciton; power dependence; temperature dependence

---

1. Introduction

Semiconductor quantum dots (QDs) are important building blocks for applications in quantum information technology where they act as qubits[1] and deterministic sources of single photons[2] or entangled photon pairs [3–6]. In this field, the QDs are usually operated at liquid helium temperature to preserve clear excitonic features in the optical spectra. But for device applications an operation at higher temperatures would be desirable to avoid expensive, large, and maintenance-intensive cooling technologies like liquid-helium cryostats or closed-cycle Gifford-McMahon (GM) systems.

However, with increasing temperature T, a broadening of the QD excitonic lines is reported as well as the formation of phonon sidebands.[7–11] Furthermore, a substantial degradation of the intensity of the emission from various types of the QDs at higher temperatures is observed.[7,8,12–18] Both effects seriously interfere with an application of QDs in optical quantum information technology at elevated temperatures.

This study focuses on GaAs cone-shell QDs (CSQDs) fabricated in a self-assembled fashion by local droplet etching[19] during molecular beam epitaxy (MBE). The self-assembled droplet etching of nanoholes into GaAs surfaces was first demonstrated by Wang et al.[20] and the fabrication of strain-free GaAs QDs by filling of droplet-etched nanoholes in AlGaAs with GaAs by us[21]. This

type of QDs demonstrates a high degree of single-photon emission and a very low neutral exciton fine-structure splitting[22] which suggests it for applications in quantum information technology[4].

The present temperature-dependent single-dot photoluminescence (PL) experiments show an only slight exciton peak broadening and only weak phonon sidebands. Even more important, the optical data establish a significant temperature enhancement of the exciton intensity with a maximum at a temperature around T = 30 K. This allows spectroscopy and possible device applications using economical and compact Stirling cryocoolers. Detailed PL measurements are performed to evaluate the temperature-dependent intensities of the exciton and biexciton peaks at varied excitation power P and for QDs with varied size. The peak intensities show a complex interplay between T- and P-dependence. For an excitation power being high enough, a rising temperature yields first an enhancement of the exciton peak intensity up to a factor of five followed by the expected reduction. For an interpretation of the data and to identify the underlying mechanisms, a model is introduced which quantitative reproduces the experimental T- and P-dependence including the temperature enhancement.

2. Experimental Setup

The fabrication of the samples with GaAs QDs embedded in an AlGaAs matrix by local droplet etching during MBE is described in previous publications[19,21]. In brief, about 30 nm deep cone-like nanoholes with a density of 2×10^7 cm^{-2} are drilled into an AlGaAs substrate (the Al content is 33 %) by self-assembled etching with Al droplets. The nanoholes are filled with GaAs for QD generation, where the thickness d_F of the GaAs filling layer controls the QD size (Figure 1a). For the present samples, the value of d_F is varied from 0.33...0.66 nm. We note that d_F is no equal to the final height of the QDs, a recent study discussing the shape and size of droplet etched QDs is given in ref. [19]. The shapes of CSQDs with the sizes discussed in the present work are calculated according to ref.[23] and shown in Figure 1b.
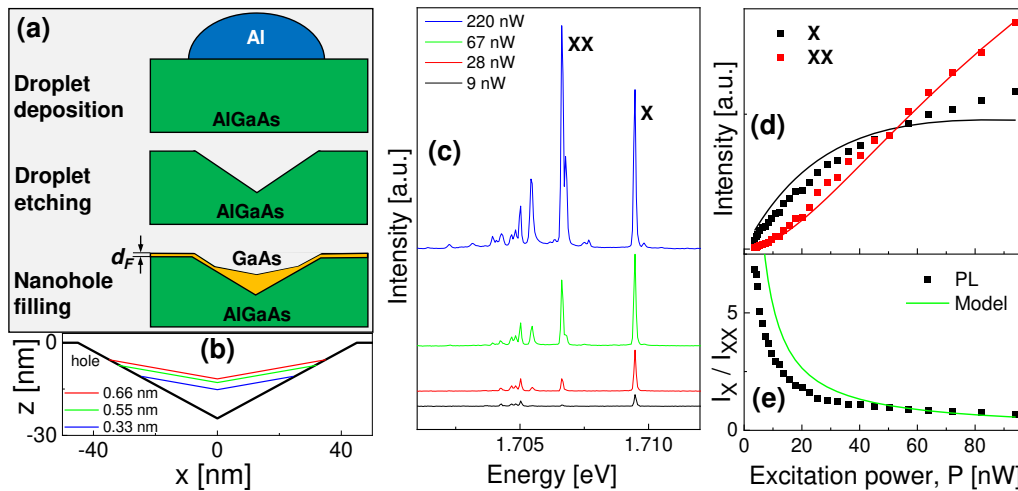

Figure 1. (a) Cross sectional sketch of the cone–shell quantum dot fabrication steps including Al droplet deposition on an AlGaAs substrate, self-assembled droplet etching of nanoholes, and filling of the nanoholes by deposition of a GaAs layer with thickness d_F; (b) Cross-sectional shape of a nanohole and of CSQDs calculated according to ref.[23] for varied d_F as indicated; (c) PL spectra from a single GaAs CSQD with d_F = 0.33 nm. The temperature is T = 3.2 K and the laser power P is varied as indicated. The exciton (X) and biexciton (XX) peaks are labeled; (d) Measured P-dependent intensities of the exciton and biexciton peaks (symbols) together with results of model calculations (lines) for a CSQD with d_F = 0.33 nm. The intensity represents the peak area of a Lorentzian fit after background subtraction; (e) Measured ratio of of the X and XX peak intensities (symbols) as function of P together with model results (line).

For the micro-PL measurements the samples are installed in an optical closed-cycle cryostat (Montana Cryostation S100), which allows a precise variation of the sample temperature from T = 3.2 K up to 350 K. For sample movement and QD selection, a stack of piezo motors is integrated inside the cryostat. The QDs are optically excited by a green (532 nm) LED laser where the laser power P is adjustable by neutral density filters. The laser power is measured with a power meter and the reading is corrected for the entrance window of the cryostat. The objective (Olympus LMPLFLN-BD, 100x0.8) for focusing the laser and collecting the light emitted from the sample is installed inside the cryostat. Due to the low QD density, individual QDs are selected without aperture by the focused laser. The QD emission is analyzed by a f=500 mm monochromator in combination with an EMCCD camera for detection.

3. Experimental Results

This section addresses measurements of the excitation power and temperature dependence of the exciton and biexcitons peak intensities from different samples with varied QD size. A model of the data is described in section 4 and a comparison between experimental and model results in section 5.

3.1. Power Dependence at Low T

Figure 1c shows typical spectra from the s-shell of a single QD taken at a low temperature (T = 3.2 K) and at a varied laser power P. We identify the peaks as follows[24,25]: the first peak arising at low P and with the highest energy is related to an exciton (one electrostatically coupled electron-hole pair). The biexciton is composed of two excitons, it has a smaller energy, and its intensity exceeds that of the exciton at higher P. The other peaks are related to charged excitons (trions) and multiexcitonic states caused by the beginning p-shell occupation. In Figure 1d an example of a measured P-dependence of the X- and XX-peak intensities is plotted and in Figure 1e the ratio of the peak intensities.

3.2. Temperature and Power Dependence

Figure 2a shows a color-coded plot of the temperature-dependent emission of a QD with d_F = 0.33 nm. The data are taken at a high P = 900 nW to increase the intensity at elevated temperatures. Due to the strong excitation, in addition to the X and XX lines also further multiexcitonic states in the s-shell and even p-shell emission are visible. The X and XX peaks are determined by P-dependent measurements as is described in section 3.1. The temperature dependent shift of the emission energies agrees with the shift of the GaAs bandgap, which means that the QD quantization energies do not depend on T. Figure 2b shows typical spectra from the same QD but now at a reduced P = 133 nW. As an important feature, the exciton intensity at T = 30 K is much higher in comparison to T = 3.2 K. This temperature enhancement is not observed for the biexciton intensity. Furthermore, the exciton peak in Figure 6c shows only weak phonon sidebands[7–11] and an only slight broadening (Figure 2c) at elevated T. We note that the low-temperature linewidth of 70 μeV represents the resolution limit of our spectrometer. In the following, the influence of T and P on the X and XX intensities is discussed in more detail.

In Figure 3 the temperature dependence of the exciton intensity I_x normalized to the intensity $I_{x,0}$ at T = 3.2 K is plotted for different QDs with varied filling layer thickness d_F measured at varied excitation power P. For an increasing temperature the data show that first $I_x/I_{x,0}$ increases up to a maximum intensity $I_{x,max}/I_{x,0}$ at a temperature $T_{x,max}$, which is followed by a strongly decreasing exciton intensity up to a complete disappearance of the signal. The unexpected increase of the intensity is explained below by an increasing excitation rate due to the onset of thermally-driven diffusion of bulk excitons from the barrier layer into the dot. The decrease above $T_{x,max}$ is explained by loss channels like bulk-exciton break-off or thermal escape of charge carriers from the QD.
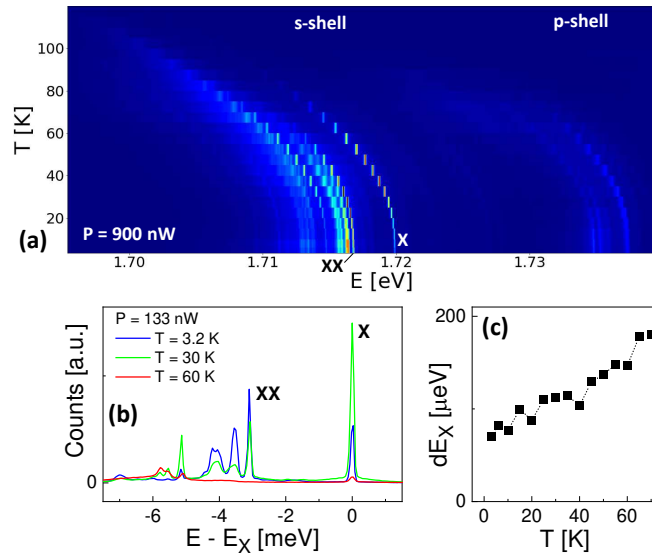
Figure 2. (a) Color-coded plot of a series of T-dependent spectra from a QD with d_F = 0.33 nm. The exciton (X) and biexciton (XX) peaks are labeled. In addition to the X and XX lines, also further multiexcitonic states in the s-shell and p-shell emission are visible due to the high excitation power of P = 900 nW. (b) Typical spectra from a QD with d_F = 0.33 nm taken at P = 133 nW and varied temperature as indicated. The energy scale is normalized to the exciton energy E_x. (c) Lorentzian linewidth of the exciton peak at P = 133 nW as function of T.

Furthermore, both $I_{x,max}/I_{x,0}$ and the corresponding $T_{x,max}$ increase with increasing excitation power. Figure 4 summarizes the maximum exciton intensity $I_{x,max}/I_{x,0}$ and the corresponding temperature $T_{x,max}$ as function of the excitation power. We see again the increase of both quantities with increasing P up to a saturation at about P = 150 nW. Regarding the QD size, there is no clear dependence of $I_{x,max}/I_{x,0}$ on d_F, whereas $T_{x,max}$ shows larger values for a smaller d_F.
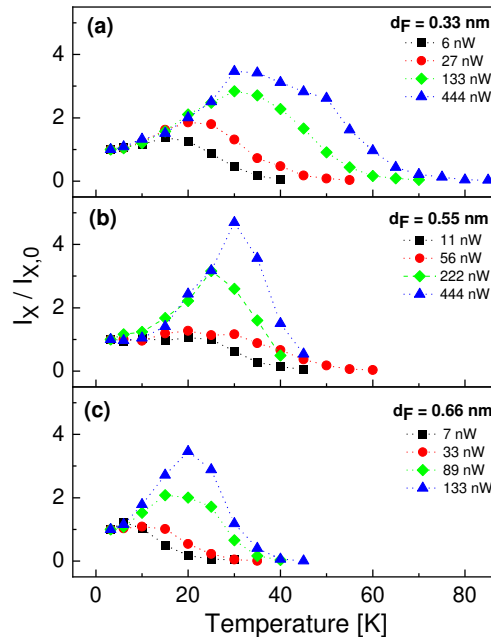

Figure 3. Temperature dependence of the exciton peak intensity I_x normalized to the intensity $I_{x,0}$ at T = 3.2 K. The intensity represents the peak area of a Lorentzian fit after background subtraction. (a)...(c) Results from different QDs with varied filling layer thickness d_F measured at the indicated excitation power P.
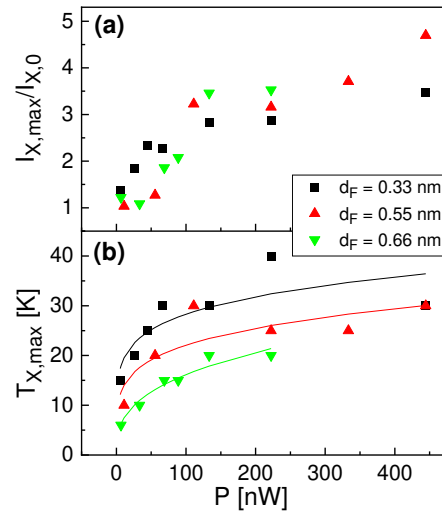
Figure 4. (a) Maximum exciton intensity $I_{x,max}/I_{x,0}$ taken from the T-dependent data in Figure 3; (b) Temperature $T_{x,max}$ of the maximum exciton intensity (symbols) together with empirical fits in the form aP^b (lines) for better visualization.

In contrast to the exciton, the biexciton intensity shows only for a high excitation power a slight increase with increasing T, at low P the intensity decreases almost directly (Figure 5). For a further analysis of this effect, Figure 6a shows the ratio of the measured exciton and biexciton intensities as function of T at varied P. Clearly visible is a strong increase of I_x/I_{xx} with increasing T and a reduction with increasing P.
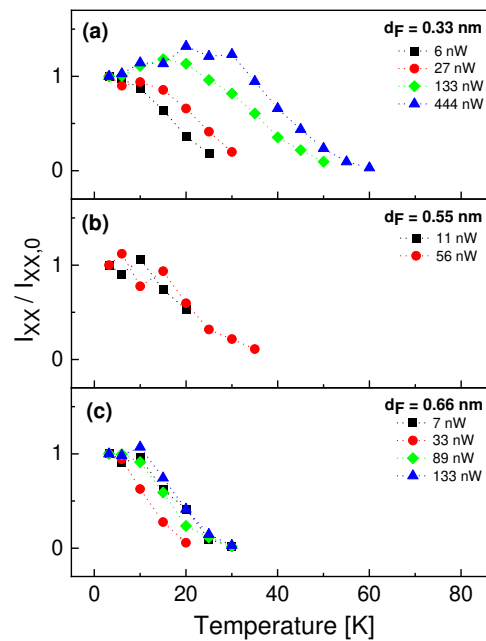

Figure 5. Temperature dependence of the biexciton peak intensity I_{xx} normalized to the intensity $I_{xx,0}$ at $T = 3.2$ K. (a)...(c) Results from different QDs with varied filling layer thickness d_F measured at the indicated excitation power P.
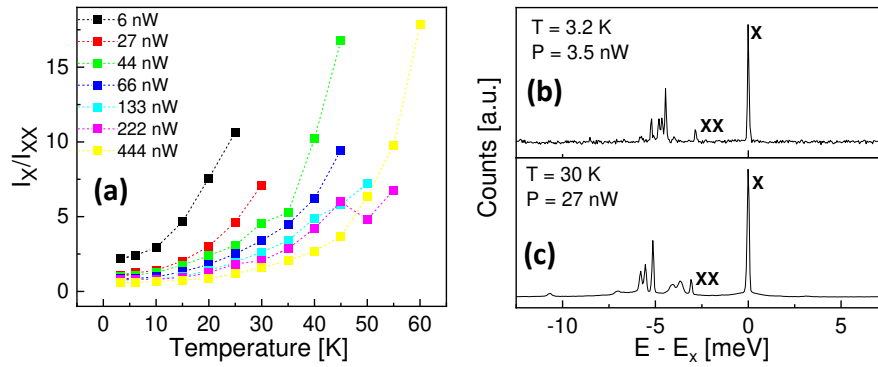
Figure 6. (a) Ratio of the measured exciton and biexciton intensities for a QD with d_F = 0.33 nm as function of T at varied P as indicated; (b) PL spectrum of a QD with d_F = 0.33 nm at T = 3.2 K and P = 3 nW; (c) PL spectrum of a QD with d_F = 0.33 nm at T = 30 K and P = 27 nW. The energy scale is normalized to the exciton energy E_x.

Figure 6b,c compare two scenarios to achieve a dominant exciton emission with $I_x/I_{xx} > 5$. The exciton and biexciton peaks are identified by their P-dependence as is described in section 3.1. The usual approach using a low temperature T = 3.2 K and a low excitation power P = 3.5 nW yields I_x/I_{xx} = 6.6 and an exciton peak linewidth of dE_x = 71 µeV. A measurement at a higher T = 30 K and P = 27 nW yields I_x/I_{xx} = 7.1 and dE_x = 109 µeV. So, the measurement a higher T maintains the peak ratio I_x/I_{xx} but broadens the linewidth by about 50%. However, we note that the accuracy of the linewidth is rather low due to the resolution limit of the spectrometer. Other artifacts like phonon sidebands are only very weak.

4. Model

The experimental data are interpreted on basis of a rate model. Starting point are the exciton and biexciton peak intensities which are described by the rate of radiative recombinations in a QD. Further considered processes are the generation of excitons by laser illumination either directly inside the QD or indirectly by diffusion from the barrier material into the dot, as well as nonradiative loss channels by bulk exciton break-off and thermal escape of excitons from a dot.

4.1. QD Peak Intensities

The QD exciton (X) and biexciton (XX) peak intensities in terms of photons per time are given by the respective rates of radiative recombinations in the QD

$$
\begin{aligned}
I_x &= c_I R_x n_x \\
I_{xx} &= c_I R_{xx} n_{xx}
\end{aligned}
\tag{1}
$$

with a constant c_I, the rates $R_x = 1/\tau_x$, $R_{xx} = 1/\tau_{xx}$ of exciton and biexciton radiative recombinations, the exciton and biexciton radiative lifetimes τ_x, τ_{xx}, and the populations n_x, n_{xx} of the exciton and biexciton states, respectively. The time-dependent populations are given by

$$
\begin{aligned}
\frac{dn_x}{dt} &= (1 - n_x - n_{xx})G - Gn_x - R_x n_x + R_{xx} n_{xx} - A n_x \\
\frac{dn_{xx}}{dt} &= Gn_x - R_{xx} n_{xx} - A n_{xx}
\end{aligned}
\tag{2}
$$

with the rate G of exciton generation in the QD and the rate A of exciton or biexciton nonradiative annihilation processes in the QD. Here, $(1 - n_x - n_{xx})G$ characterizes the generation of excitons in non-occupied dot states, Gn_x the exciton to biexciton transformation, $R_x n_x$, $R_{xx} n_{xx}$ the excition and

biexciton radiative decay, and An_x, An_{xx} exciton and biexciton nonradiative annihilation processes. In equilibrium ($t \rightarrow \infty$, $dn_x/dt = dn_{xx}/dt = 0$) we get

$$
\begin{aligned}
n_x &= \frac{(R_{xx} + A)G}{A^2 + A(2G + R_x + R_{xx}) + G^2 + GR_{xx} + R_xR_{xx}} \\
n_{xx} &= \frac{G}{R_{xx} + A}n_x
\end{aligned}
\tag{3}
$$

4.2. Exciton Generation

As the central approach to explain the temperature-enhancement of the QD exciton emission, we assume that a QD collects excitons by direct generation inside the dot plus additional bulk excitons that diffuse from the barrier material into the dot:

$$
G = G_q + G_d,
\tag{4}
$$

where G_q is the rate of direct exciton generation inside a QD and G_d the rate of exciton diffusion from the barrier material into a dot.

The laser illumination with power P means a flux of $n_{ph,0} = c_pP$ photons per unit of time and volume element towards the sample surface, with a constant c_P. The photon flux is attenuated inside the AlGaAs barrier material which is described following the Lambert-Beer law $n_{ph}(x) = n_{ph,0}\exp(-\alpha x)$, with the depth x below the surface, $n_{ph,0} = n_{ph}(x = 0) = c_pP$, and the absorption coefficient $\alpha = 55930$ cm^{-1} (AlGaAs with an Al content of 0.315 at a laser wavelength of 532 nm [26]). In an undoped semiconductor, light is mainly absorbed by the formation of excitons. This gives the depth profile of the exciton generation rate $Q(x) = -dn_{ph}(x)/dx = \alpha\exp(-\alpha x)c_pP$. Assuming a spherical QD with a radius $r_0 = 5$ nm which is located $d = 80$ nm below the surface, the rate of direct exciton generation in a QD becomes

$$
G_q = (4/3)\pi r_0^3 Q_0 = (4/3)\pi r_0^3 c_\alpha c_P P,
\tag{5}
$$

with $Q_0 = Q(d + r_0) = c_\alpha c_P P$ and $c_\alpha = \alpha\exp(-\alpha[d + r_0]) = 0.00348$ nm.

To evaluate the diffusion of excitons from the barrier material into a dot, we apply the approximation that the direct exciton generation rate inside a QD and in the surrounding barrier material is constant and equals Q_0. Far away from the dot, the density of bulk excitons in the barrier material is $n_{b,0}/dt = Q_0 - n_{b,0}R_b - n_{b,0}A_b$, with the rate R_b of bulk exciton radiative recombinations and the rate A_b at which bulk excitons are annihilated by thermal break-off. In equilibrium ($t \rightarrow \infty$, $n_{b,0}/dt = 0$) we get $n_{b,0} = Q_0/(R_b + A_b)$. For the bulk exciton radiative decay in AlGaAs we assume a lifetime $\tau_b = 1/R_b = 1$ ns[27] and for the annihilation of bulk excitons by thermal break-off we assume a rate $A_b = \nu_{A,b}\exp[-E_{A,b}/(k_BT)]$, where $\nu_{A,b}$ is a prefactor, $E_{A,b}$ an activation energy, and k_B Boltzmann's constant. We introduce now the diffusion of excitons from the barrier material into a QD that is treated like a spherical sink with radius r_0. In steady-state the rate at which excitons diffuse towards the dot is $J = 4\pi r^2 Ddn_b/dr$, with the diffusion coefficient $D = \nu_D\exp[-E_D/(k_BT)]$, the prefactor ν_D, the activation energy E_D, and the radial distance r to the QD center at $r = 0$. This is solved by $n_b(r) = n_{b,0} - J/(4\pi rD)$. With the boundary condition $n_b(r_0) = 0$ at the QD surface, we get $J = 4\pi r_0 Dn_{b,0}$. Now, the rate of indirect exciton generation in a QD by exciton diffusion from the barrier becomes

$$
G_d = 4\pi r_0^2 J = (4\pi)^2 r_0^3 Dn_{b,0} = (4\pi)^2 r_0^3 Dc_\alpha c_P P/(R_b + A_b).
\tag{6}
$$

4.3. Exciton Annihilation

Two mechanisms for the annihilation of generated excitons are considered. The thermal break-off in the barrier material is described already above in section 4.2. In addition, exciton annihilation can take place by thermal escape of charge carriers from a QD (see eqns. 2 and 3), which is already

addressed in ref. [18]. The rate of thermal escape is described by $A = \nu_A \exp[-E_A/(k_B T)]$, where ν_A is a prefactor and E_A an activation energy. Of course there are other possible exciton loss-channels like Auger processes[28]. However these are neglected here since we do not expect a strong temperature dependence.

5. Model Results

This section addresses the application of the model for the interpretation of the experimental PL data.

5.1. Power Dependence at Low T

At low $T = 3.2$ K, several approximations can be applied to the model of eqn. 3. In detail, the thermally activated loss channels A and the diffusion coefficient D for indirect exciton generation are negligible small which yields $G = G_q$. This simplifies eqn. 3 to

$$
\begin{aligned}
n_{x,0} &= \frac{G_q R_{xx}}{(R_x + G_q) R_{xx} + G_q^2} \\
n_{xx,0} &= \frac{G_q}{R_{xx}} n_{x,0}
\end{aligned}
\tag{7}
$$

Equations 1 and 7 allow the calculation of the X and XX power dependencies and a comparison with the experimental data in Figure 1b using four free model parameters c_I, c_P, R_x, and R_{xx}. To reduce the number of free parameters, we consider previous lifetime measurements[19] of similar QDs which indicate $\tau_x = 1/R_x = 0.39$ ns for $d_F = 0.33$ nm. The remaining parameters are determined by fitting: $\tau_{xx} = 1/R_{xx} = 0.068$ ns, $c_P = 0.0265$ ns^{-1}nW^{-1}nm^{-2}, and $c_I = 226$.

Figure 1d shows a comparison of the model results with the experimental data at low $T = 3.2$ K. Despite its simplicity, the model demonstrates a good reproduction of the power dependence of I_x and I_{xx}. Also the power dependence of the intensity ratio I_x/I_{xx} is well reproduced by the model (Figure 1e), where eqn. 7 predicts $I_x/I_{xx} = R_x/G$. However, we note that the fitted value of τ_{xx} is unrealistic small. In a simple approximation it can be assumed that $\tau_{xx} = \tau_x/2 = 0.145$ ns, since a biexciton with a doubled number of charge carriers has a doubled recombination rate in comparison to a single exciton. The inaccuracy of the fitted τ_{xx} can be related to the influence of states in higher shells that are not considered in the model.

5.2. Temperature and Power Dependence

The temperature dependence of the normalized exciton intensity in Figure 3 is modeled by $I_x/I_{x,0}$, where $I_x = c_I R_x n_x$ (eqn. 3) considers the temperature dependence and $I_{x,0} = c_I R_x n_{x,0}$ (eqn. 7) the intensity at low temperature $T = 3.2$ K, as is addressed above in section 5.1. We use the model parameters $c_I = 226$, $c_P = 0.0265$ ns^{-1}nW^{-1}nm^{-2}, as well as $\tau_x = 0.39$ ns and $\tau_{xx} = \tau_x/2 = 0.145$ ns according to section 5.1. Due to the number of remaining model parameters, the fitting is done in several steps.

In a first step, the bulk exciton diffusion related parameters $\nu_D = 3.2 \times 10^8$ s^{-1} and $E_D = 4.2$ meV are determined for best agreement with the approximately exponential growth of $I_x/I_{x,0}$ in the temperature range of $T = 3.2 \ldots 30$ K. In a next step, the bulk exciton break-off related parameters $\nu_{A,b} = 2.22 \times 10^{11}$ s^{-1} and $E_{A,b} = 20.5$ meV are fitted in the temperature range of $T = 3.2 \ldots 50$ K. And finally, the parameters $\nu_A = 3.22 \times 10^{15}$ s^{-1} and $E_A = 72$ meV describing the thermal escape are fitted over the whole temperature range. Figure 7a visualizes the respective regimes at which the different processes have an influence and demonstrates the very good reproduction of the experimental temperature-dependence by the model.
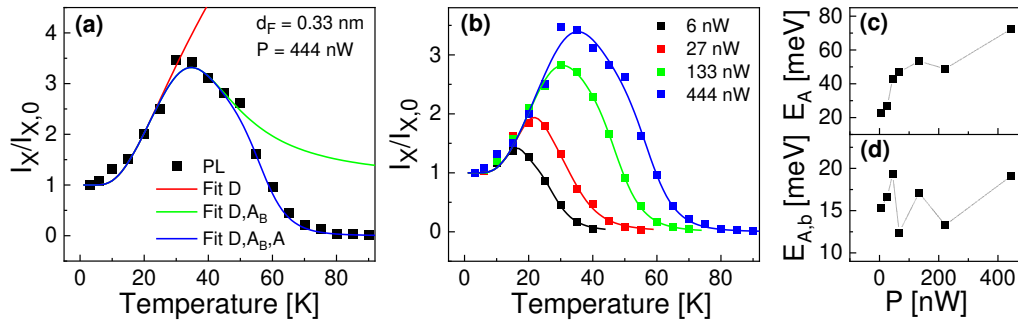
Figure 7. Normalized exciton intensity $I_x/I_{x,0}$ as function of T. (a) Comparison of experimental (PL) values with model results, where the processes considered in the model are varied. All model calculations include exciton generation in the QD (Q_q) and radiative recombinations R_x, R_{xx}. Fit D considers in addition exciton diffusion from the barrier into the QD, Fit D, A_b also bulk exciton break-off, and Fit D, A_b, A also thermal escape of charge carriers from a dot; (b) Comparison of experimental (symbols) and calculated (lines) values at varied laser power P as indicated; (c),(d) Fitted exciton-annihilation related activation energies as function of P.

However, as a significant difference to the experimental behavior (Figure 3), the model shows almost no influence of the excitation power P on the normalized exciton intensity $I_x/I_{x,0}$. Mathematically, this is caused by the normalization, where two quantities with similar P-dependence are divided. Obviously, the mechanism for the experimental P-dependence is not included in the model. Since the slope of the bulk exciton diffusion related increase does not depend on P (Figure 3a), we assume here an additional P-dependence of either the bulk exciton break-off or the thermal escape. To test this, we have fitted the exciton-annihilation related parameters for other values of P. The resulting activation energies $E_{A,b}$ for bulk exciton break-off and E_A for thermal escape are plotted in Figure 7c. There, the values of E_A show a clear increase with P, whereas $E_{A,b}$ is almost constant. We assume a mechanism where exciton annihilation by thermal escape is caused by a combination of several thermally activated processes, with the respective strengths being controlled by the excitation power.

6. Discussion and Conclusions

The temperature dependence of the exciton and biexciton peak intensities from GaAs cone-shell QDs is studied at varied excitation power and dot size. An interesting finding is a strong temperature enhancement of the exciton emission up to a factor of five. The maximum intensity and the corresponding temperature $T_{x,max}$ depend on excitation power and dot size. The experimental data are modeled by considering the competing processes of exciton generation, annihilation, and recombination. Exciton generation in the QDs takes place by direct excitation in the dot layer plus additional bulk excitons that diffuse from the barrier layers into the dot. The temperature-dependent bulk-exciton diffusion is the reason for the temperature-enhanced exciton emission. Above $T_{x,max}$, the intensity decreases due to exciton annihilation processes. In comparison to the exciton, the biexciton intensity shows an only very weak enhancement, which is attributed to a more efficient annihilation.

A temperature enhancement was also reported for the optical emission from GaAs quantum wells embedded in an AlGaAs barrier.[27] There, the enhancement was related to the same mechanism as depicted in the present study, i.e., generation of excitons also in the barrier material and their temperature-driven diffusion into the quantum wells. Considering this mechanism, a temperature enhancement of the exciton intensity under nonresonant excitation is expected for all types of QDs which are embedded in a thick semiconductor barrier. Such epitaxial QDs are usually fabricated by MBE. Nevertheless, the literature which provides T-dependent PL data on various types of single epitaxial QDs[7,8,13,15,16] reports no temperature enhancement. Only in ref. [17] a slight temperature enhancement is observed for InAs/GaAs multilayer QDs. However, these measurements are done using ensemble PL, which integrates the whole s-shell intensity including charged excitons and

multiexcitonic lines and allows no clear relation to the pure exciton intensity. According to Figure 4, a probable reason for the absence of a temperature enhancement is a very low excitation power P, which is often used in the literature for studies focusing on the exciton behavior.

From a practical point of view, the enhancement of the exciton intensity can substantially simplify the spectroscopy of single QDs. A $T_{x,max}$ around 30 K allows to substitute the usual expensive, large, and maintenance-intensive sample-cooling technologies (liquid-helium or closed-cycle Gifford-McMahon cryostats) which is required for the spectroscopy at liquid helium temperature. With a base temperature around 30 K, spectroscopy of excitonic features becomes now possible by inexpensive and compact Stirling cryocoolers with a long Mean Time To Failure (MTTF). The usage of Stirling cryocoolers also simplifies the development of devices for quantum information technology, where single QDs are utilized as a single-photon source[15]. On the other side, studies including the behavior of biexcitons are suggested at liquid-helium temperature, since the biexciton intensity shows an only very weak temperature enhancement and significantly degrades at elevated temperatures.

References

1. Vasconcellos, S.M.d.; Gordon, S.; Bichler, M.; Meier, T.; Zrenner, A. Coherent control of a single exciton qubit by optoelectronic manipulation. *Nature Photonics* **2010**, *4*, 545–548. https://doi.org/10.1038/nphoton.2010.124.

2. Somaschi, N.; Giesz, V.; Santis, L.D.; Loredo, J.C.; Almeida, M.P.; Hornecker, G.; Portalupi, S.L.; Grange, T.; Antón, C.; Demory, J.; et al. Near-optimal single-photon sources in the solid state. *Nature Photonics* **2016**, *10*, 340–345. https://doi.org/10.1038/nphoton.2016.23.

3. Keil, R.; Zopf, M.; Chen, Y.; Höfer, B.; Zhang, J.; Ding, F.; Schmidt, O.G. Solid-state ensemble of highly entangled photon sources at rubidium atomic transitions. *Nature Communications* **2017**, *8*, 15501. https://doi.org/10.1038/ncomms15501.

4. Huber, D.; Reindl, M.; Huo, Y.; Huang, H.; Wildmann, J.S.; Schmidt, O.G.; Rastelli, A.; Trotta, R. Highly indistinguishable and strongly entangled photons from symmetric GaAs quantum dots. *Nature Communications* **2017**, *8*, 15506. https://doi.org/10.1038/ncomms15506.

5. Arakawa, Y.; Holmes, M.J. Progress in quantum-dot single photon sources for quantum information technologies: A broad spectrum overview. *Applied Physics Reviews* **2020**, *7*, 021309. https://doi.org/10.1063/5.0010193.

6. Lodahl, P.; Ludwig, A.; Warburton, R.J. A deterministic source of single photons. *Physics Today* **2022**, *75*, 44–50. https://doi.org/10.1063/PT.3.4962.

7. Besombes, L.; Kheng, K.; Marsal, L.; Mariette, H. Acoustic phonon broadening mechanism in single quantum dot emission. *Physical Review B* **2001**, *63*, 155307. https://doi.org/10.1103/PhysRevB.63.155307.

8. Abbarchi, M.; Gurioli, M.; Vinattieri, A.; Sanguinetti, S.; Bonfanti, M.; Mano, T.; Watanabe, K.; Kuroda, T.; Koguchi, N. Phonon sideband recombination kinetics in single quantum dots. *Journal of Applied Physics* **2008**, *104*, 023504. https://doi.org/10.1063/1.2948932.

9. Denning, E.V.; Iles-Smith, J.; Gregersen, N.; Mork, J. Phonon effects in quantum dot single-photon sources. *Optical Materials Express* **2020**, *10*, 222–239. https://doi.org/10.1364/OME.380601.

10. Abbarchi, M.; Mano, T.; Kuroda, T.; Sakoda, K. Exciton Dynamics in Droplet Epitaxial Quantum Dots Grown on (311)A-Oriented Substrates. *Nanomaterials* **2020**, *10*, 1833. https://doi.org/10.3390/nano10091833.

11. Wigger, D.; Karakhanyan, V.; Schneider, C.; Kamp, M.; Höfling, S.; Machnikowski, P.; Kuhn, T.; Kasprzak, J. Acoustic phonon sideband dynamics during polaron formation in a single quantum dot. *Optics Letters* **2020**, *45*, 919–922. https://doi.org/10.1364/OL.385602.

12. Jing, P.; Zheng, J.; Ikezawa, M.; Liu, X.; Lv, S.; Kong, X.; Zhao, J.; Masumoto, Y. Temperature-Dependent Photoluminescence of CdSe-Core CdS/CdZnS/ZnS-Multishell Quantum Dots. *The Journal of Physical Chemistry C* **2009**, *113*, 13545–13550. https://doi.org/10.1021/jp902080p.

13. Tighineanu, P.; Daveau, R.; Lee, E.H.; Song, J.D.; Stobbe, S.; Lodahl, P. Decay dynamics and exciton localization in large GaAs quantum dots grown by droplet epitaxy. *Physical Review B* **2013**, *88*, 155320. https://doi.org/10.1103/PhysRevB.88.155320.

14. Jagtap, A.M.; Khatei, J.; Rao, K.S.R.K. Exciton–phonon scattering and nonradiative relaxation of excited carriers in hydrothermally synthesized CdTe quantum dots. *Physical Chemistry Chemical Physics* **2015**, *17*, 27579–27587. https://doi.org/10.1039/C5CP04654H.

15. Schlehahn, A.; Krüger, L.; Gschrey, M.; Schulze, J.H.; Rodt, S.; Strittmatter, A.; Heindel, T.; Reitzenstein, S. Operating single quantum emitters with a compact Stirling cryocooler. *Review of Scientific Instruments* **2015**, *86*, 013113. https://doi.org/10.1063/1.4906548.

16. Yuan, Q.; Liang, B.; Zhou, C.; Wang, Y.; Guo, Y.; Wang, S.; Fu, G.; Mazur, Y.I.; Ware, M.E.; Salamo, G.J. Interplay Effect of Temperature and Excitation Intensity on the Photoluminescence Characteristics of InGaAs/GaAs Surface Quantum Dots. *Nanoscale Research Letters* **2018**, *13*, 387. https://doi.org/10.1186/s11671-018-2792-y.

17. Abiedh, K.; Zaaboub, Z.; Hassen, F.; David, T.; Sfaxi, L.; Maaref, H. Experimental and theoretical study of thermally activated carrier transfer in InAs/GaAs multilayer quantum dots. *Applied Physics A* **2020**, *126*, 491. https://doi.org/10.1007/s00339-020-03654-8.

18. Ranasinghe, L.; Heyn, C.; Deneke, K.; Zocher, M.; Korneev, R.; Hansen, W. Luminescence from Droplet-Etched GaAs Quantum Dots at and Close to Room Temperature. *Nanomaterials* **2021**, *11*, 690. https://doi.org/10.3390/nano11030690.

19. Heyn, C.; Gräfenstein, A.; Pirard, G.; Ranasinghe, L.; Deneke, K.; Alshaikh, A.; Bester, G.; Hansen, W. Dot-Size Dependent Excitons in Droplet-Etched Cone-Shell GaAs Quantum Dots. *Nanomaterials* **2022**, *12*, 2981. https://doi.org/10.3390/nano12172981.

20. Wang, Z.M.; Liang, B.L.; Sablon, K.A.; Salamo, G.J. Nanoholes fabricated by self-assembled gallium nanodrill on GaAs(100). *Applied Physics Letters* **2007**, *90*, 113120–113122. https://doi.org/10.1063/1.2713745.

21. Heyn, C.; Stemmann, A.; Köppen, T.; Strelow, C.; Kipp, T.; Grave, M.; Mendach, S.; Hansen, W. Highly uniform and strain-free GaAs quantum dots fabricated by filling of self-assembled nanoholes. *Applied Physics Letters* **2009**, *94*, 183113–183115. https://doi.org/10.1063/1.3133338.

22. Küster, A.; Heyn, C.; Ungeheuer, A.; Juska, G.; Tommaso Moroni, S.; Pelucchi, E.; Hansen, W. Droplet etching of deep nanoholes for filling with self-aligned complex quantum structures. *Nanoscale Research Letters* **2016**, *11*. https://doi.org/10.1186/s11671-016-1495-5.

23. Heyn, C.; Ranasinghe, L.; Deneke, K.; Alshaikh, A.; Duque, C.A.; Hansen, W. Strong Electric Polarizability of Cone–Shell Quantum Structures for a Large Stark Shift, Tunable Long Exciton Lifetimes, and a Dot-to-Ring Transformation. *Nanomaterials* **2023**, *13*, 857. Number: 5 Publisher: Multidisciplinary Digital Publishing Institute, https://doi.org/10.3390/nano13050857.

24. Heyn, C.; Strelow, C.; Hansen, W. Excitonic lifetimes in single GaAs quantum dots fabricated by local droplet etching. *New Journal of Physics* **2012**, *14*, 053004–053015. https://doi.org/10.1088/1367-2630/14/5/053004.

25. Graf, A.; Sonnenberg, D.; Paulava, V.; Schliwa, A.; Heyn, C.; Hansen, W. Excitonic states in GaAs quantum dots fabricated by local droplet etching. *Physical Review B* **2014**, *89*, 115314. https://doi.org/10.1103/PhysRevB.89.115314.

26. Aspnes, D.E.; Kelso, S.M.; Logan, R.A.; Bhat, R. Optical properties of AlGaAs. *Journal of Applied Physics* **1986**, *60*, 754–767. https://doi.org/10.1063/1.337426.

27. Jiang, D.S.; Jung, H.; Ploog, K. Temperature dependence of photoluminescence from GaAs single and multiple quantum-well heterostructures grown by molecular-beam epitaxy. *Journal of Applied Physics* **1988**, *64*, 1371–1377. https://doi.org/10.1063/1.341862.

28. Efros, A.L.; Nesbitt, D.J. Origin and control of blinking in quantum dots. *Nature Nanotechnology* **2016**, *11*, 661–671. https://doi.org/10.1038/nnano.2016.140.